Renewable and Sustainable Energy Reviews 205 (2024) 114843

Contents lists available at ScienceDirect

Renewable and Sustainable Energy Reviews

journal homepage: www.elsevier.com/locate/rser

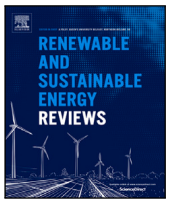

Original research article

Order of magnitude increase in power from flow-induced vibrations

Jonathan C.C. Lo [a,*], Mark C. Thompson [a], Kerry Hourigan [a], Jisheng Zhao [a,b]

[a] Fluids Laboratory for Aeronautical and Industrial Research (FLAIR), Department of Mechanical and Aerospace Engineering, Monash University, Clayton, 3800, Victoria, Australia

[b] School of Engineering and Technology, University of New South Wales, Canberra, 2600, ACT, Australia

ARTICLE INFO

Keywords:
Flow-structure interactions
Flow-induced vibration
Vortex shedding
Hydro-power
Renewable energy sources

ABSTRACT

Natural hydro environments such as rivers and ocean currents provide abundant and essentially free sources of kinetic energy. Although significant research has been devoted to harnessing this power through traditional turbine systems, there are also studies on the novel use of flow-induced vibration of a bluff body. The large oscillations of an elliptical cylinder resulting from the newly-discovered hyper branch have raised interesting questions about its potential as a source of effective renewable energy. This study investigates the power extraction characteristics of the hyper branch over a range of flow velocities. A factor-of-ten increase in the maximum time-mean power coefficient relative to an established flow-induced vibration system — the vortex induced vibration for aquatic clean energy converter is demonstrated. This suggests the possibility of a new and effective strategy to utilise flow-induced vibrations for energy generation and could help drive the commercial implementation and uptake of oscillating energy converters.

1. Introduction

With many of the world-largest industrial countries pledging that their nations will be carbon-neutral by mid-century [1], the need for more novel and effective methods of generating energy from the natural environment has never been greater. As significant quantities of free kinetic energy can be found in fluid flows, numerous approaches to harvest these power sources have been devised [2–5]. Such methods often include the use of rotary turbines to extract tidal energy [2,3], or the application of devices like buoys and water columns to harvest power from oscillations on the water surface [4,5]. However, common methods like tidal barrages cause detrimental disturbances to the local marine environment and are also expensive to construct [6], whilst the drawback for surface oscillation-based generators is the potentially narrow operational range of oscillation frequencies in which optimal performance can be achieved [7,8]. To overcome some of these disadvantages, the use of vortex-induced vibration (VIV) of a circular cylinder as a new technique of renewable energy extraction was proposed [9]. VIV, an extensively studied type of flow-induced vibration (FIV) [10,11], is the product of fluctuating hydrodynamic forces acting on the body caused by the shedding of vortices into the wake in a cyclic pattern known as a von Kármán vortex street. A phenomenon associated with VIV is wake-body synchronisation, whereby the vortex shedding frequency "locks in" to the oscillation frequency over an extended range of flow velocities [12,13]. The resultant device, named the VIVACE (vortex induced vibration for aquatic clean energy) converter [9], seeks to maximise the power production from the structural vibration by allowing the elastically-mounted cylinder to freely oscillate transversely to the flow. The strengths of this device are its robustness, increased operational range and modularity.

However, the VIVACE converter can only utilise VIV for energy harvesting due to the axial symmetry of a circular cylinder. As VIV is self-limited (i.e. with the maximum achievable oscillation amplitude being limited to the order of one cylinder diameter), vibrations become insignificant at high flow speeds. Consequently, a significant number of studies has been conducted into different modifications to the geometry and configuration of the oscillating bluff body to improve the maximum power extracted as well as to expand its operational flow speed range [14–16]. This can be achieved by inducing galloping, which is a typical FIV phenomenon that can maintain significant structural vibration at high reduced flow velocity and is experienced by cylindrical bodies with aerodynamically unstable cross-sections [10,17]. Unlike VIV, galloping is instead driven by a movement-induced instability arising from an asymmetric pressure distribution due to changes in the instantaneous flow incidence angle as the body translates in the fluid. Since this results in the aerodynamic forces being in line with and favouring the body movement velocity, larger oscillation amplitudes can be attained and are typically present for all flow speeds above a certain critical threshold [17]. For the circular cylinder, galloping can be instigated by attaching passive turbulence control (PTC) devices in

* Corresponding author.
E-mail address: jonathan.lo1@monash.edu (J.C.C. Lo).

https://doi.org/10.1016/j.rser.2024.114843
Received 9 October 2023; Received in revised form 14 August 2024; Accepted 18 August 2024
Available online 26 August 2024

Nomenclature

Abbreviations

CNC	Computerised numerical control
DOF	Degrees of freedom
FIV	Flow-induced vibration
Hyper-ACE	Hyper branch aquatic clean energy
PTC	Passive turbulence control
VIV	Vortex-induced vibration
VIVACE	Vortex induced vibration for aquatic clean energy

Symbols

A^*	Normalised oscillation amplitude
A^*_{10}	Top 10% of A^* over the measurement period
a	Streamwise diameter of elliptical cylinder
b	Cross-flow diameter of elliptical cylinder
c	Damping coefficient
C_p	Power coefficient
$\overline{C}_p$	Time-averaged power coefficient
C_y	Transverse force coefficient
f	Oscillation frequency
f_{na}	Natural frequency in quiescent air
$f_{\mathrm{na}}{}^*$	Normalised natural frequency in quiescent air
f_{nw}	Natural frequency in quiescent water
F_y	Cross-flow fluid force
k	Spring constant
m	Mass of oscillating system
m_f	Displaced fluid mass
m^*	Mass ratio
Re	Reynolds number
S	Projected area of cylinder onto cross-flow plane
T	Oscillation period
T_M	Measurement period
U_∞	Freestream velocity
U^*	Reduced velocity
y	Body displacement
y^*	Normalised body displacement
$\dot{y}$	Body velocity
$\ddot{y}$	Body acceleration
L	Immersed length of cylinder
ε	Elliptical ratio of cylinder
ζ	Damping ratio
ν	Kinematic viscosity of water
ρ	Density of water

the form of roughness strips, or thin cylindrical rods onto the cylinder surface. There has also been significant research into harnessing the FIV of other prismatic bodies such as cylinders with square [18,19], semi-circular [20], and triangular [21] cross sections. Therefore, the introduction of galloping to the FIV response of a bluff body is shown to increase the overall performance of FIV-based energy converters. Further details can be found in previous literature reviews [15,16].

Beyond the utilisation of a single cylinder, increases in power production could also be realised by utilising multiple cylinder elements arranged as part of an energy harvester assembly [22]. In the case of energy harvesting from water flows, it has been shown that the inclusion of multiple cylinders improved the energy harvesting performance over a solitary cylinder for the circular [23], diamond and square [24], and triangular [25] cross sections. Of note, Kim and Bernitsas [26] found that multiple circular cylinders with PTC attachments can work together synergistically, thereby harvesting more energy than the same number of single cylinders in isolation.

Whilst previous studies have focused on investigating the power extraction performance of common prismatic bodies (e.g. circular and square cross sections), research on energy harvesting from elliptical cylinders appears limited. Herein, the cross-sectional profile of an elliptical cylinder is described by the elliptical ratio $\varepsilon = b/a$, where a and b are the stream-wise and cross-flow (transverse) dimensions, respectively. The literature has demonstrated that the vibration is amplified when $\varepsilon > 1$ [27], with enhancement reported by Shi et al. [28] in the piezoelectric energy harvesting of an elliptical cylinder of $\varepsilon = 2.5$ compared to the circular cylinder. While investigating the effect of structural damping on the cross-flow FIV of an elliptical cylinder of $\varepsilon = 5$, Lo et al. [29] have recently shown a region of large vibration (i.e. amplitudes up to approximately $8b$) corresponding to the joint occurrence of both VIV and a movement-induced instability with similarities to galloping. Coined the hyper branch, they demonstrated that substantial oscillations in this region could indeed be maintained for significant structural damping. Additionally, since the large oscillations of the hyper branch can be excited at low flow speeds with higher-frequency oscillations compared to traditional galloping currently reported for other geometries in the literature, this distinguishing behaviour highlights the unexplored promise of thin elliptical cylinders as an effective and high-power output geometry for energy extraction.

Here, this research builds upon the works of Bernitsas et al. [9] and Lo et al. [29] by proposing a new concept called the hyper branch aquatic clean energy (Hyper-ACE), which demonstrates the viability of the hyper branch as an FIV-based technique for energy generation. Utilising the FIV of an elliptical cylinder and an electromagnetic damper system to simulate the loads applied by a generator, the resultant power coefficient was used to compare the performance achieved in this study with other state-of-the-art FIV-based energy converters. Due to the presence of large oscillations even with significant damping, the thin elliptical geometry enhanced the power coefficient of the VIVACE converter by a maximum of almost 900% (see Section 4.4). This improvement in performance could make Hyper-ACEs a commercially attractive proposition for power harvesting from slow water currents.

2. Theoretical background

2.1. Fluid–structure system model

When considering power generation, the hyper branch response under the external loading provided by an energy generator must first be explored. To study this hydrodynamic phenomenon, an elastically mounted elliptical cylinder with an elliptical ratio of $\varepsilon = 5$, as illustrated by the schematic in Fig. 1(a), is used. Approximating this oscillator system as a linear second-order mass–spring–damper model, the fluid forcing can be calculated from the governing equation of motion:

$$F_y(t) = m\ddot{y} + c\dot{y} + ky, \tag{1}$$

where m is the oscillating mass, c is the damping coefficient and k is the spring constant. This system can hence be characterised with respect to the following non-dimensional parameters: the mass ratio ($m^* = m/m_f$, with m_f being the displaced fluid mass), Reynolds number ($\mathrm{Re} = Ub/\nu$), damping ratio ($\zeta = c/(2\sqrt{km})$), reduced velocity ($U^* = U/(f_{\mathrm{nw}}b)$), and normalised displacement ($y^* = y/b$, with the mean of the top 10% of the normalised amplitude peaks denoted by A^*_{10}). The characteristic length is the cylinder width projected on the axis of vibration (i.e. y), which in this study is b. Here, where m is the total oscillating mass, m_f is the

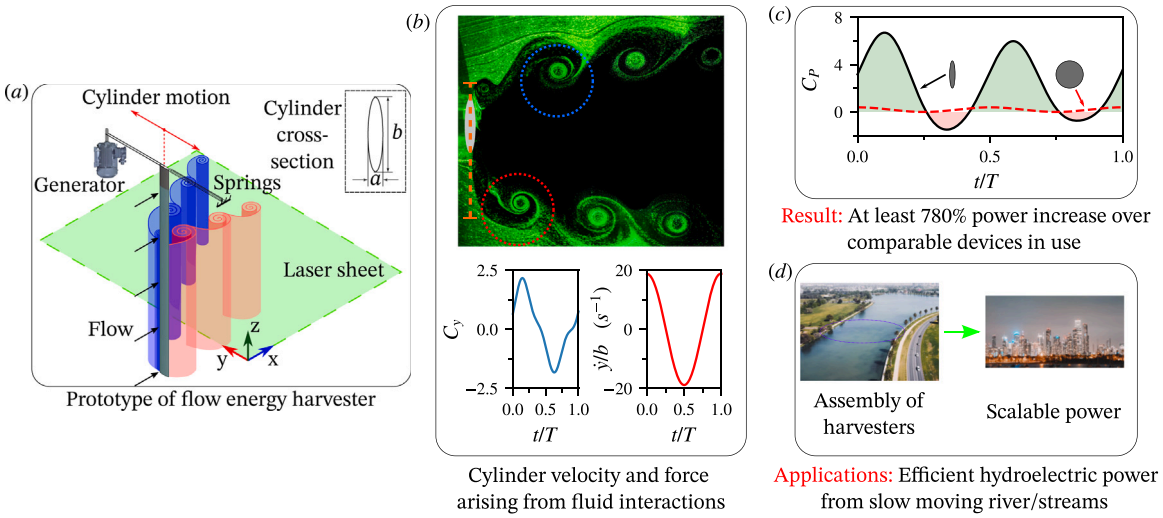

Fig. 1. Schematic of the approach and key findings of this study. (*a*) Simplified schematic of the elastically mounted but freely-vibrating cylinder system. The loads applied by a generator during energy conversion are simulated through the damping applied to the structure via the electromagnetic damper mechanism [30], with the full description of the experimental set-up found in Section 3. (*b*) The dynamics of the cylinder (bottom: fluid forcing and velocity of the cylinder over one oscillation cycle) due to vortex shedding (top: two-dimensional visualisation of the wake with the laser sheet of (*a*) as the light source) that arise from the fluid–structure interaction. (*c*) The product of fluid forcing and velocity leads to a net power extraction from the fluid flow, which is 780% higher than devices that utilise the FIV of a circular cylinder [30]. (*d*) Potential applications of this research as an effective and non-invasive alternative for energy generative from slow-moving water flows.

mass of the fluid displaced by the cylinder, ν is the kinematic viscosity of the flow at the conditions in which the tests are conducted, and f_{nw} is the natural oscillation frequencies when the system is in quiescent water.

2.2. Power and efficiency of energy harvesting from FIV

The standard methodology for measuring and comparing the power extraction from FIV is through non-dimensionalisation of the power output with respect to the free-stream energy passing through the projected area onto the cross-flow plane (i.e. the y–z plane). In line with the studies of Bernitsas et al. [9] and Soti et al. [30], the area is taken as $S = bL$, where L is the immersed length of the cylinder in the spanwise direction. Thus, the non-dimensional instantaneous power as a function of time t is defined in this study as the power coefficient ($C_p(t)$):

$$C_p(t) = \frac{P(t)}{\frac{1}{2}\rho U_\infty^3 S} = \frac{F_y(t)\cdot\dot{y}(t)}{\frac{1}{2}\rho U_\infty^3 S} = \frac{C_y(t)\cdot\dot{y}(t)}{U_\infty}, \tag{2}$$

where ρ is the fluid density and U_∞ is the freestream velocity; $P(t)$ is the instantaneous power transferred from the flow to the freely oscillating cylinder, and is the product of the cylinder's movement speed $\dot{y}$ and the total force acting on the cylinder by the fluid $F_y(t)$; and $C_y(t) = F_y(t)/(\frac{1}{2}\rho U_\infty^2 S)$ is the non-dimensional transverse force coefficient. As damping is equivalent to the structural load applied by a generator, the rate of energy extraction from the fluid flow by the oscillating body is hence directly proportional to the magnitude of the applied damping as well as to the velocity of the body motion. It is noted that in other fields, non-dimensionalisation is done with respect to the swept area (henceforth referred to as the efficiency η), with this difference further discussed in Section 4.2.

As identified using Eq. (2), the time-mean power shown in Fig. 1(*b*–*c*) depends on $\dot{y}(t)$ and $F_y(t)$, which are in turn determined by the interaction between the elastically-mounted cylinder and the fluid. The FIV response can hence be affected by varying the flow conditions or the structural properties. Since the primary goal of this study is to ascertain the energy harvesting performance of the elliptical geometry, the parameters of interest are the flow speed and the structural damping. In these experiments, the former parameter was varied by controlling the flow rate in the water-channel facility used, and the structural damping was controlled via an electromagnetic damper developed by Soti et al. [30]. Details of the water channel facility and damper device used can be found in Section 3.

2.3. Analytical expression for energy harvesting

To understand the interplay between the experimental parameters that leads to the highest time-averaged power extraction from the hyper branch instability, an analytical solution to integrating over Eq. (2) with respect to time must first be developed. As a result of the almost purely sinusoidal nature of the hyper branch oscillations, this study assumes that the displacement is well-approximated by the form $y^* = A^* \sin(2\pi f t)$, where f is the oscillation frequency. From this assumption, both $\dot{y}(t)$ and $y(t)$ both have an absolute phase difference of 90° to $\dot{y}(t)$ and, as such, do not contribute to the dot product when the expression for $F_y(t)$ from Eq. (1) is substituted into Eq. (2). The integral equation, after appropriate non-dimensionalisation, becomes:

$$\overline{C}_P = \frac{1}{T_M}\int_t^{t+T_M} \frac{c\,\dot{y}(t)\cdot\dot{y}(t)}{\frac{1}{2}\rho U_\infty^3 bL}\,dt = \frac{4\pi^4}{\varepsilon}\zeta {f_{\mathrm{na}}}^* {f^*}^2 m^* \left(\frac{A^{*2}}{U^{*3}}\right). \tag{3}$$

Here T_M is the measurement period, and $f^* = f/f_{\mathrm{nw}}$ and ${f_{\mathrm{na}}}^* = f_{\mathrm{na}}/f_{\mathrm{nw}}$ are the oscillation frequency and natural frequency of the cylinder in quiescent air normalised by the natural frequency of the system in quiescent water, respectively.

3. Experimental procedures

3.1. Elastically mounted cylinder system

The bluff body investigated in this study was a smooth rigid elliptical cylinder manufactured from aluminium using precision computerised numerical control (CNC) machining and hard anodised surface treatment against water corrosion. The cylinder has an immersed length of $L = 614$ mm, and streamwise and cross-flow diameters of $a = 5$ mm and $b = 25$ mm, respectively. To ensure that the system is freely oscillating in the crossflow direction, the top end of the cylinder was mounted on the support carriage of a low-friction air-bearing system which was positioned above the water channel. Further details on the air-bearing system used in this study can be found in Zhao et al. [31,32]. The structural stiffness of this hydroelastic system was provided by

stainless-steel extension springs attached to both sides of the carriage whilst variable damping was applied using the electromagnetic damper device developed by Soti et al. [30]. With the damper device consisting of a stationary conductive copper plate placed at a distance from a permanent magnet mounted directly onto the carriage, the desired damping value can be achieved by varying this gap. For this study, the structural damping range of interest spanned $3.65 \times 10^{-3} \leqslant \zeta \leqslant 1.90 \times 10^{-1}$. Therefore, the total oscillating mass including the cylinder, magnet, and carriage, equals $m = 1046.4$ g. The displaced mass was calculated as $m_f = \rho \pi abL/4 \approx 60$ g and resulted in a mass ratio of $m^* \approx 17.4$. The method and experimental approach have been further detailed by Lo et al. [29].

The natural frequency and damping ratio parameters in this study were obtained by first conducting free decay tests in both quiescent air and water. In free decay testing, the oscillating body is released after being displaced by some known distance from its equilibrium position and the resultant time traces of the freely vibrating system are used to calculate the parameters. Further mathematical details can be found in Blevins [10] and Sumer et al. [33].

3.2. Flow conditions

The experiments were conducted in the recirculating free-surface water channel in the Fluids Laboratory for Aeronautical and Industrial Research (FLAIR) at Monash University. The test section of the water channel has a width, depth, and length of 600 mm, 800 mm and 4000 mm, respectively. The turbulence level of the resultant free-stream was less than 1%, and well-known empirical relationships were used to obtain the kinematic viscosity and density of the fluid from temperature measurements. Parallel vortex shedding of the cylinder was encouraged by placing a conditioning platform on the channel floor with an approximately 1 mm gap between the bottom of the cylinder and the platform [see34]. The Reynolds numbers and reduced velocities of interest were $990 \leq \mathrm{Re} \leq 4390$ and $U^* \in [2.3,10]$, respectively, which corresponds to a maximum flow speed range of $U = 40.5–178.9$ mm/s. To characterise the power extraction of the Hyper-ACE system, the structural response of the elliptical cylinder was examined as a function of reduced velocity for the range of damping ratios of interest in this study. While keeping the damping fixed, the flow velocity was swept in U^* increments of either 0.05 or 0.1, with experiments conducted using both increasing and decreasing increment directions to ascertain if any hysteretic effects were present.

3.3. Data acquisition

Both data acquisition and control of the flow speed were automated through a customised LabVIEW (National Instruments, USA) software. Measurements were obtained with an USB DAQ device (model: USB6218-BNC, National Instruments, US) sampling at 100 Hz for $T_M = 300$ s. Transverse displacement was measured using a non-contact digital optical linear encoder (model RGH24; Renishaw, UK) with a total range of 400 mm at a resolution of 1 μm, whilst the temperature was recorded using a resistance temperature detector (RTD) sensor (Model: P-M-1/10-1/8-6-1/8-P-3, Omega Engineering Limited, USA) with an interchangeability of 0.03 °C. Given the resolution of the optical linear encoder, the transverse force F_y (which is required to measure the power coefficient in Eq. (2)) was hence determined via Eq. (1) where the required velocity and acceleration terms are calculated through the numerical differentiation of the displacement signal. Validations of this method can be found in [32,35].

4. Results

4.1. Energy harvesting performance of the hyper branch

The effect of the damping ratio on the time-mean power coefficient ($\overline{C_P}$) and non-dimensionalised structural vibration amplitude (A^*_{10}) are first established over a range of reduced velocities in order to ascertain the conditions that will yield the possible highest power output from the elliptical cylinder. Though the full data set is further discussed in Section 4.3, the time-averaged power curve corresponding to the highest observed maximum power coefficient as a function of reduced velocity for fixed damping ratios is presented in Fig. 2. The highest power coefficient with fixed damping is $\max\{\overline{C}_P\} = 2.93$ (occurring for damping ratio of $\zeta = 1.91 \times 10^{-2}$ and reduced velocity of $U^* = 7.50$). As will be discussed in Section 4.4, further increases in power ($\overline{C}_p = 3.31$) can also be achieved if the initial conditions are appropriately selected.

To appreciate the significant improvement in performance with this Hyper-ACE concept, its power coefficient is also plotted for comparison with the VIVACE converter (with and without surface modifications), as well as other energy generators based on cross-flow FIV of non-circular bluff bodies. Table 1 provides a summary of the maximum $\overline{C}_P$ values reported in the literature. Since this research assumes that the transverse fluid force exerted on the system by the hyper branch instability is completely converted into power, the reported $\overline{C}_P$ values here can be interpreted as the upper limit or maximum power that can be extracted using hyper branch oscillations (for a given U^* and ζ) without considering losses during the conversion from kinetic to useable electrical energy. However, for commercial development of such energy converters, inefficiencies that reduce the true power output may include electrical resistance in the wiring and frictional forces in the mechanical components of the device.

The hyper branch response in this study has shown an increase of almost 800% in the maximum $\overline{C}_P$ compared to that of $\overline{C}_P = 33.23\%$ experimentally achieved by Lee and Bernitsas [36] for a single VIVACE module (with the further factor-of-ten increase in performance demonstrated in Section 4.4), and a 671% increase when compared to the theoretical upper limit calculated by Bernitsas et al. [9]. As illustrated in Fig. 2, this increase is also representative of other singular transversely oscillating bluff bodies. Furthermore, it should be noted that the maximum of $\overline{C}_P = 0.200$ obtained by Soti et al. [30] for a circular cylinder is still approximately 6.9% of the maximum value reported in this study. As their results were obtained under similar experimental conditions (i.e. at a similar Reynolds number of $Re = 5330$ and using the same electromagnetic damper), this highlights the substantial enhancement in $\overline{C}_P$ achieved in this study.

Although galloping could be induced for circular cylinders via modifications or additional structures onto the cylinder surface [14,37], it did not produce substantially large amplitudes at low reduced velocities as observed in Fig. 2 of this study. As such, whilst the galloping response can extend the reduced velocity range in which meaningful power can be extracted, the increase in the maximum $\overline{C}_P$ is much less than that observed for this hyper branch response. Referring to Eq. (3), this difference is due to the large vibration occurring at a lower reduced velocity and an oscillation frequency that is $f^* \approx 1$, whilst the large vibration occurs at a higher reduced velocity and at a lower frequency (i.e. $f^* < 1$) for galloping [14]. Of the bluff bodies investigated by Tamimi et al. [21], the triangular cross-section produced the highest power coefficient $\overline{C}_P = 0.145$. As galloping is mainly responsible for the amplitude response induced by this geometry, it further illustrates the power extraction performance of the hyper branch (arising from the joint occurrence of VIV and a galloping-like movement-induced instability) superior over the purely galloping responses reported in the literature.

Due to the similarity of the elliptical cylinder profile (in the cross-flow direction) to those of airfoils, further comparisons can also be drawn from the energy extraction of “flapping” airfoils with fully

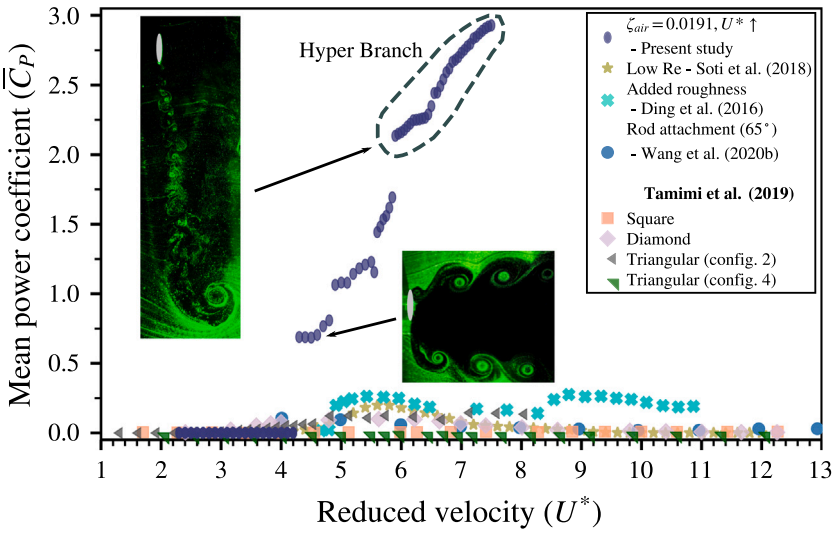

Fig. 2. A comparison of the time-averaged power coefficients for different bluff body geometries over a range of reduced velocities $U^* = U_\infty/(f_{nw}b) \in [1, 13]$, where f_{nw} is the natural frequency of the system in quiescent water. For this study, the power curve with the highest observed maximum power coefficient is shown and corresponds to a fixed damping ratio of $\zeta_{air} = 0.0191$ with the flow velocity increased continuously from the minimum to the maximum speed (denoted by $U^* \uparrow$). The representative wake structures shed by the oscillating elliptical cylinder, visualised using hydrogen bubbles, are shown as insets. The vibrational amplitude responsible for this power response can be found in Fig. 3(*a*). The symbols denoting the results of Tamimi et al. [21] and this study also represent the shape and orientation of the cylinders relative to a flow from left to right.

Table 1
Summary of the maximum time-mean power coefficients for different geometries and FIV systems obtained from the literature.

Study	Method	Geometry	Mass (m^* or kg)	Crossflow diameter (mm)	Re	Max $\overline{C}_P$ (%)
This Study	Experiment (Water)	**Elliptical cylinder** (from rest) (externally excited, see Section 4.4)	17.4	25	990–4390	 293 331
Lee and Bernitsas [36]	Experiment (Water)	**Circular cylinder**	8.88 kg	88.9	40,000–120,000	33
Soti et al. [30]	Experiment (Water)	**Circular cylinder**	3	30	2220–6661	20.0
Ding et al. [14]	2D simulation (Water)	**Circular cylinder** (+ roughness strips)	1.896	88.9	30,000–110,000	28
Wang et al. [37]	2D simulation (Water)	**Circular cylinder** (+ rods 65°apart)	1.6774	88.9	35,000–115,000	10.6
Tamimi et al. [21]	Experiment (Water)	**Square cylinder** **Diamond cylinder** **Triangular cylinder** (2nd config) **Triangular cylinder** (4th config)	1.69 1.69 2.7 2.7	50 70.71 70.71 50	2325–27,129 4384–40,011 4384–38,366 3100–29,454	0.95 10.0 14.5 1.05
Wang et al. [38]	2D simulation (Water)	**Flapping airfoil** (NACA 0012)	2.0	–	400	95
Kinsey and Dumas [39]	2D simulation (Water)	**Flapping airfoil** (NACA 0015)	–	–	1100	113

passive two degrees of freedom (two-DOF) in heaving and pitching motions. In their numerical simulations, Kinsey and Dumas [39] reported a maximum $\overline{C}_P$ of 1.13, while 0.95 was obtained in Wang et al. [38]. Of significant interest, the maximum power coefficient $\overline{C}_P = 2.93$ presented in Fig. 3 shows a significant increase of greater than 159%. Furthermore, the simplicity of this one-DOF elliptical cylinder is advantageous over the two-DOF flapping airfoils in that the additional degree of freedom of flapping devices also adds complexity to the system, thereby increasing their manufacturing and maintenance costs and reducing their robustness and effectiveness in real-world applications.

4.2. Measuring energy harvesting performance

It is important to note that efficiency has been purposely neglected thus far in the assessment of the hyper branch as an alternative source of FIV energy harvesting. Often defined as the generated power divided by power (available) in the fluid volume swept out by the vibration of the bluff body, the efficiency can be mathematically represented by:

$$\eta = \frac{P_{\text{generated}}}{P_{\text{fluid}}} = \frac{P_{\text{generated}}}{\frac{1}{2}\rho U_\infty^3 Lb(1+2A^*)} = \frac{\overline{C}_P}{1+2A^*}. \quad (4)$$

where $Lb(1 + 2A^*)$ is the total swept area by the cylinder during one oscillation period.

For cross-flow FIV-based energy harvesters such as the one proposed here, Eq. (4) shows that the efficiency will decrease with non-dimensional amplitude if the rate at which $\overline{C}_P$ increases is outpaced by the increase in A^*. With greater energy generated from larger oscillations, this places hyper branch-based energy converters at a distinct disadvantage for direct comparison to horizontal-axis turbines whose swept area remains constant. As this study only investigates the power

extraction from FIV of a single elliptical cylinder with $2A^* \gg 0$, the small fluid volume being utilised for energy generation at any given point of the vibration leads to a maximal efficiency of $\eta = 22.7\%$. This is approximately 38.3% of the theoretical efficiency limit for an ideal rotor turbine ($\eta = 59.26\%$) as indicated by Betz's law, with commercial horizontal axis wind turbines reaching around 70%–80% of this limit [40,41]. As Betz derived this upper bound from one-dimensional momentum theory, the result also applies to cross-flow FIV energy harvesters.

However, with this study primarily focusing on the potential energy extraction properties of a single thin elliptical cylinder (with the large power coefficient achieved due to the magnitude of hyper branch oscillations sustained by the body), the efficiency parameter does not reflect the true performance of the newly discovered hyper branch. Drawing parallels to wind turbines, the empirical equations developed by Wilson et al. [42] show that larger efficiencies can be gained from increasing the number of turbine blades. Of course, the efficiency of a wind turbine increases as the number of blades is increased, so having a system of multiple freely-vibrating elliptical cylinders that are placed either in parallel or in tandem relative to the flow can be hypothesised to increase overall efficiency. This concurs with the study by Kim and Bernitsas [26], who showed that increasing the number of circular cylinders (with passive turbulence control devices attached) also improved the efficiency of the VIVACE converter system. A peak efficiency of 88.6% with respect to the Betz limit was achieved when four cylinders were placed in tandem, noting that the Betz's efficiency for a single circular cylinder is approximately 25%. Furthermore, the hydrodynamic interference effect of multiple freely-vibrating cylinders will induce wake-induced vibration and wake-coupled vibration for the tandem and side-by-side configurations, respectively. As shown in the review by Wang et al. [43] that both phenomena result in the amplification of the oscillation amplitude for the circular geometry when compared to a single isolated cylinder, similar effects may arise that increase the vibration amplitude and hence power generation for multiple freely-vibrating thin elliptical cylinders. As such, the efficiency term alone cannot fully describe the power extraction performance without also considering a system of multiple cylinders.

4.3. Implication of effect of damping on energy harvesting

Whilst the variation of $\overline{C}_P$ as a function of U^* was discussed in Section 4.1, the shape of this response is sensitive to the structural damping ratio and the direction in which U^* was varied, as can be observed in Fig. 3. Therefore, two tests were conducted for each damping ratio such that the first experiment was taken when the flow speed was increased continuously in positive increments from the minimum to the maximum, whereas the direction was reversed for the second experiment. These tests are respectively denoted by $U^* \uparrow$ and $U^* \downarrow$.

In line with the definitions proposed by Lo et al. [29], the hyper branch in this study is the discontinuous linear response region above $A^*_{10} \approx 4$, as shown in Fig. 3(a). It consists of two sections: a soft-start regime where substantial body vibration can be induced from rest in the flow, and a hard-start regime where a large initial displacement is needed to trigger the hyper branch oscillations to occur. Both regions can be respectively identified by the agreement and divergence of the $U^* \uparrow$ and $U^* \downarrow$ curves. When ζ increases beyond 1.94×10^{-2}, the substantially large hyper branch oscillations are attenuated and the amplitude response becomes generally continuous. Lo et al. [29] attributes this behaviour to the joint occurrence of VIV and movement-induced instability present in the hyper branch since the large body oscillations of the hyper branch cause a small angle between the incident flow and the semi-major axis, $\alpha = \arctan(\dot{y}/U_\infty)$. The cylinder's elongated profile in the direction of motion and the lack of sharp corners that could induce flow separation enhance flow attachment over the lateral sides of the body. Additionally, the thin elliptical cross-section effectively function akin to an airfoil, contributing to the movement-induced instability in FIV dynamics. The latter is evidenced by the hydrogen-bubble inset of the hyper branch in Fig. 2, which shows the presence of a secondary von Kármán vortex street (independent of the main singular counter-clockwise vortex shown at the bottom of the image) shed by the cylinder during its motion. Consequently, the airfoil-like behaviour of the thin ellipse thereby increases the net transverse fluid force (equivalent to the difference between the components of positive lift and negative drag acting in the y direction) exerted on the body as it translates across the flow. Therefore, the hyper branch has significant energy harvesting implications, given that the large oscillations sustained by the elliptical cylinder (even when significant structural damping is applied) are responsible for the power coefficients observed in this study. As such, the peak power coefficient curve shown in Fig. 2 corresponds to the largest damping ratio that could still sustain the hyper branch ($\zeta = 1.91 \times 10^{-2}$) when positive U^* increments are used.

To understand the significant energy harvesting performance of the thin elliptical cylinder geometry, the time traces in Fig. 4 show the evolution of the measured normalised displacement and the instantaneous power coefficient over several periods of hyper branch oscillations. As an overwhelming majority of the energy is imparted by the water flow to the cylinder, this means that on average, substantial positive work can be extracted from the hyper branch oscillations. It should be noted that for all the amplitude responses of $U^* \uparrow$ in Fig. 3(a), the hyper branch oscillation amplitudes could reach the limit of the experimental set-up ($A^* \approx 8$ in Fig. 3a) before the maximum U^* was reached. Referring to Eq. (3), it is hence very likely that higher $\overline{C}_P$ values can be observed at greater U^* values with oscillation amplitudes beyond the limits of the experimental set-up.

4.4. Effect of initial displacement on the power characteristics of the hyper branch

As previously discussed, the presence of the hyper branch is dependent on the initial transverse movement of the elliptical cylinder. Since the results of Fig. 3 are produced with the oscillating system initially at rest, different behaviours can be observed if the cylinder is externally excited into the hyper branch. With this change to the initial conditions, Fig. 5 shows the variations of $\overline{C}_p$ and A^*_{10} as a function of ζ for a range of fixed reduced velocities. Instead of maintaining a fixed ζ value and varying U^* as is the case for Fig. 3, the ζ range is slowly swept from lower to higher values until the hyper branch eventually disappears. An advantage of this experiment is that the lower ζ bound can be adjusted to ensure the oscillations are within the limits of the experimental setup, thus allowing for higher U^* values to be investigated.

From Fig. 5(b), the highest power coefficient value is $\overline{C}_P = 3.31$ (observed for $\zeta = 2.88 \times 10^{-2}$ at $U^* = 8.50$), an increase of 12.9% over the maximum value produced by the fixed ζ experiments in Fig. 3. This also corresponds to an almost factor-of-ten enhancement in the maximum $\overline{C}_P$ as compared to the VIVACE converter of Lee and Bernitsas [36]. Interestingly, while the ceiling of ζ can be considered as the critical damping ratio (i.e. the highest damping ratio that the hyper branch can sustain in this study) and covers a range of $\zeta \in [0.273, 0.300]$, it differs from the critical value reported for Fig. 3 due to the variation in initial conditions between the two experiments. The delay in the critical value reported in Fig. 5 can be attributed to the hyper branch being driven by a movement-induced instability in combination with VIV, resulting in greater damping ratios required to attenuate a system already undergoing hyper branch oscillations as compared with one starting initially from rest.

Overall, the enhancement in the maximum $\overline{C}_P$ shown here indicates that providing an initial amplitude to excite the oscillating cylinder into the hyper branch can assist in maximising the power extraction, especially for situations where oscillation amplitudes are constrained below a certain limit. Once the hyper branch oscillations are established, variable damping can then be used as a control strategy to delay the maximum U^* in which the hydrodynamic instability can be

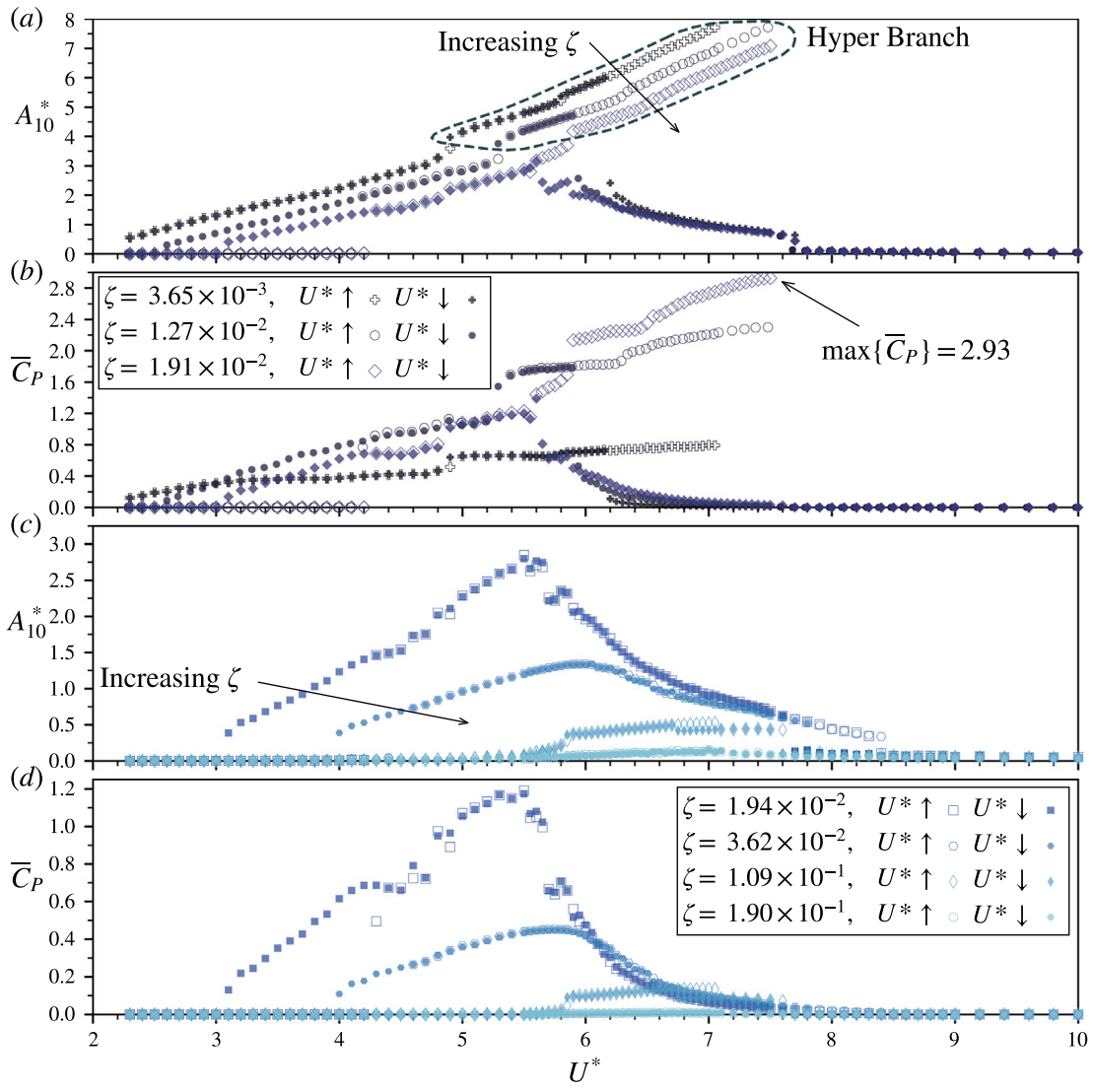

Fig. 3. Normalised oscillation amplitude A_{10}^* and corresponding time-mean power coefficient $\overline{C_p}$ for various damping ratios ζ are compared over a range of reduced velocities U^*. (a, b) The hyper branch is present for $\zeta \geq 0.0191$ whilst it is suppressed (c, d) below this critical damping ratio. The flow speed is changed in a constant direction for a given trial, either sequentially increased ($U^*\uparrow$) or decreased ($U^*\downarrow$). The amplitude responses of (b, d) are taken from Lo et al. [29].

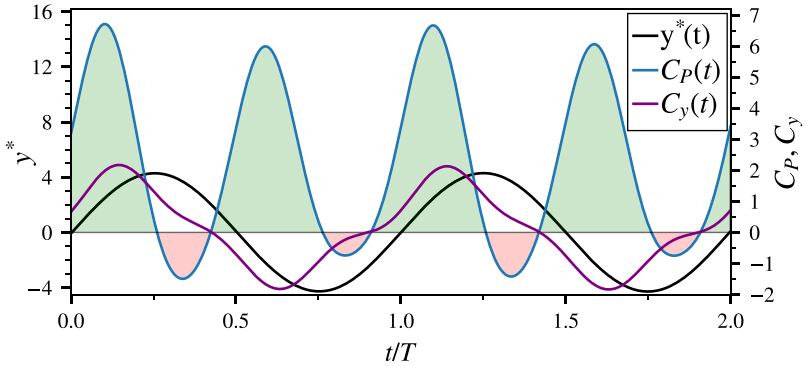

Fig. 4. The measured time trace of the normalised displacement (black), power coefficient (blue), and the transverse force coefficient (purple) over two oscillation periods (i.e. $2T$) at a damping ratio of $\zeta = 1.91\times10^{-2}$ and reduced velocity of $U^* = 6.00$. The green and red shadings of $C_P(t)$ indicate the positive and negative contributions to integrating Eq. (2) over time, respectively.

sustained for a given transverse width of a system. By preserving the large vibrations even at high U^* values, this approach will increase the operational range and peak power coefficients from the hyper branch response.

It is important to note that the $\overline{C}_P$ values in Fig. 5 can be affected by environmental changes and the experimental procedure. These factors include the temperature and depth of the water, the rate at which ζ is adjusted between data points, as well as the initial hyper branch

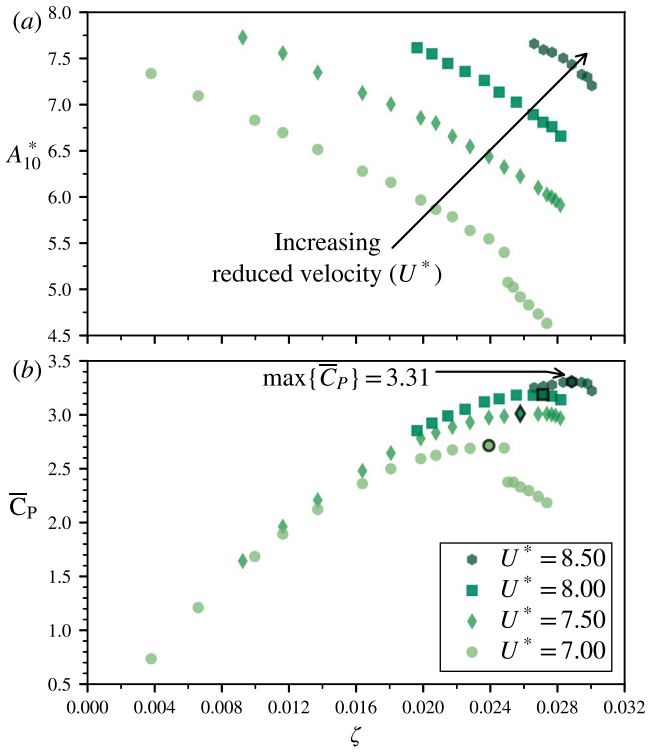

Fig. 5. (*a*) The amplitude and (*b*) the time-mean power coefficient response of the freely-vibrating cylinder for different reduced velocities are compared over a range of damping ratios. The system is initially excited into the hyper branch at the minimum ζ for a given trial with measurements taken as damping is increased. The maximum $\overline{C}_p$ observed for each reduced velocity is highlighted with a black symbol outline in (*b*). For all the reduced velocities tested, the power coefficient drops as ζ approaches the critical damping value (i.e. maximum damping that can still sustain the hyper branch).

oscillation amplitude at the beginning of the tests. However, these effects can be considered negligible since the trials for the same U^* value are similar in trend, with the maximum $\overline{C}_P$ value at the critical damping ratio varying by less than 2%. To minimise these effects on the comparison, the data set shown in the figure was collected on the same day under almost identical experimental conditions. In addition, the data set was specifically presented as it was the lower bound of observed power coefficients, thereby providing a conservative estimate of the energy harvesting performance.

5. Discussion and conclusion

The results of this study have shown an approximately factor-of-ten increases in $\overline{C}_P$ from Hyper-ACE over other FIV-based energy harvesters in the literature. The greater energy generation potential produced by the hyper branch response with substantially large vibration to be sustained over significant damping ratios and lower reduced velocities. Since this proposed energy extraction method relies on the cross-flow FIV and builds upon the VIV-based method first proposed by Bernitsas et al. [9], the advantages of the VIVACE converter also apply here as well. Additionally, due to the significantly lower Reynolds number values required to sustain the hyper branch response, optimal energy generation can hence occur at slower flow speeds or for smaller-size harvesters.

However, for the practical implementation of this newly discovered hyper branch, further research should explore the potential for harvesting useable power by replacing the electromagnetic damper utilised in this study with a generator. Additionally, different approaches to maximise the power extraction performance and improve its robustness to marine environment variability in real-world sites should also be the subject of further development. First, the effect of having multiple elliptical cylinders either in a side-by-side or tandem configuration can also be considered for further gains in efficiency. As such, the optimal spacing between, and the number of, cylinders required must be ascertained to harness the additional interference effects that arise from the interactions between the wakes of multiple cylinders [43]. Second, unlike the laminar and constant flows generated in this study, currents in marine environments are often turbulent and temporally varying in nature. As such, future work should explore control optimisation measures to sustain these oscillations for a wide range of flow conditions. For example, flow speed fluctuations can have a detrimental effect on power production performance given the dependence of the hyper branch on the initial vibrational amplitude. Embedding a system that injects the system with kinetic energy to initiate and maintain hyper branch oscillations, as well as implementing a variable-load inductor that in real-time ensures both optimal power generation and that oscillations are within the physical limits of the system, should be the subject of further investigation. Finally, modifications to the surface of the cylinder can also be utilised to promote FIV. By placing additional structures and optimising their locations on the elliptical cylinder surface, further enhancements, similar to the improvements observed for the VIVACE converter [see 14,37,44], in the vibration amplitude and the range of flow velocities for which the oscillations occur may be achieved.

In this study, it has been demonstrated the exceptional power generation potential of the hyper branch instability for an elastically mounted elliptical cylinder freely vibrating with one degree of freedom. Along with extending this body of work to the development of an energy-input device to initiate the hyper branch, future improvements to the proposed system should also explore the benefits of including more cylinder elements (either in parallel or in tandem) and modifying the surface topology of the cylinder to maximise the performance of future Hyper-ACE-based devices.

CRediT authorship contribution statement

Jonathan C.C. Lo: Conceptualization, Data curation, Formal analysis, Investigation, Methodology, Software, Writing – original draft. **Mark C. Thompson:** Conceptualization, Project administration, Resources, Supervision, Writing – review & editing. **Kerry Hourigan:** Conceptualization, Funding acquisition, Supervision, Writing – review & editing. **Jisheng Zhao:** Conceptualization, Funding acquisition, Methodology, Project administration, Resources, Supervision, Writing – review & editing.

Declaration of competing interest

The authors declare that they have no known competing financial interests or personal relationships that could have appeared to influence the work reported in this paper.

Data availability

Data will be made available on request.

Acknowledgements

This work is supported by the Australian Research Council Discovery Early Career Researcher Award [grant number DE200101650]; and the Australian Research Council Discovery Project [grant number DP210100990].

References

[1] Deutch J. Is net zero carbon 2050 possible? Joule 2020;4(11):2237–40.
[2] Khan M, Bhuyan G, Iqbal M, Quaicoe J. Hydrokinetic energy conversion systems and assessment of horizontal and vertical axis turbines for river and tidal applications: A technology status review. Appl Energy 2009;86(10):1823–35.
[3] Güney M, Kaygusuz K. Hydrokinetic energy conversion systems: A technology status review. Renew Sustain Energy Rev 2010;14(9):2996–3004.
[4] Falcão AFO. Wave energy utilization: A review of the technologies. Renew Sustain Energy Rev 2010;14(3):899–918.
[5] Clemente D, Rosa-Santos P, Taveira-Pinto F. On the potential synergies and applications of wave energy converters: A review. Renew Sustain Energy Rev 2021;135:110162.
[6] Rourke FO, Boyle F, Reynolds A. Tidal energy update 2009. Appl Energy 2010;87(2):398–409.
[7] Guo B, Ning D, Wang R, Ding B. Hydrodynamics of an oscillating water column WEC - Breakwater integrated system with a pitching front-wall. Renew Energy 2021;176:67–80.
[8] Zhao XL, Ning DZ, Zou QP, Qiao DS, Cai SQ. Hybrid floating breakwater-WEC system: A review. Ocean Eng 2019;186:106126.
[9] Bernitsas MM, Raghavan K, Ben-Simon Y, Garcia EMH. VIVACE (Vortex Induced Vibration Aquatic Clean Energy): A new concept in generation of clean and renewable energy from fluid flow. J Offshore Mech Arct Eng 2008;130(4):041101.
[10] Blevins RD. Flow-induced vibration. 2nd ed. New York, NY (USA): Van Nostrand Reinhold Inc.; 1990.
[11] Bearman PW. Vortex shedding from oscillating bluff bodies. Annu Rev Fluid Mech 1984;16(1):195–222.
[12] Govardhan R. Vortex-induced vibrations. Annu Rev Fluid Mech 2004;36:413–55.
[13] Sarpkaya T. A critical review of the intrinsic nature of vortex-induced vibrations. J Fluids Struct 2004;19(4):389–447.
[14] Ding L, Zhang L, Bernitsas MM, Chang C-C. Numerical simulation and experimental validation for energy harvesting of single-cylinder VIVACE converter with passive turbulence control. Renew Energy 2016;85:1246–59.
[15] Wang J, Geng L, Ding L, Zhu H, Yurchenko D. The state-of-the-art review on energy harvesting from flow-induced vibrations. Appl Energy 2020;267:114902.
[16] Lv Y, Sun L, Bernitsas MM, Sun H. A comprehensive review of nonlinear oscillators in hydrokinetic energy harnessing using flow-induced vibrations. Renew Sustain Energy Rev 2021;150:111388.
[17] Naudascher E, Rockwell D. Flow-induced vibrations: An engineering guide. Dover; 2005.
[18] Han P, Huang Q, Pan G, Wang W, Zhang T, Qin D. Energy harvesting from flow-induced vibration of a low-mass square cylinder with different incidence angles. AIP Adv 2021;11(2).
[19] Wang J, Gu S, Abdelkefi A, Zhang M, Xu W, Lai Y. Piezoelectric energy harvesting from flow-induced vibrations of a square cylinder at various angles of attack. Smart Mater Struct 2021;30(8):08LT02.
[20] Sun W, Zhao D, Tan T, Yan Z, Guo P, Luo X. Low velocity water flow energy harvesting using vortex induced vibration and galloping. Appl Energy 2019;251:113392.
[21] Tamimi V, Armin M, Shahvaghar-Asl S, Naeeni STO, Zeinoddini M. FIV Energy Harvesting From Sharp-Edge Oscillators. In: International conference on offshore mechanics and arctic engineering, vol. 58899. American Society of Mechanical Engineers; 2019, p. V010T09A001.
[22] Fan X, Guo K, Wang Y. Toward a high performance and strong resilience wind energy harvester assembly utilizing flow-induced vibration: Role of hysteresis. Energy 2022;251:123921.
[23] Sui G, Shan X, Tian H, Wang L, Xie T. Study on different underwater energy harvester arrays based on flow-induced vibration. Mech Syst Signal Process 2022;167:108546.
[24] Tamimi V, Esfehani MJ, Zeinoddini M, Naeeni STO, Wu J, Shahvaghar-Asl S. Marine hydrokinetic energy harvesting performance of diamond and square oscillators in tandem arrangements. Energy 2020;202:117749.
[25] Shao N, Lian J, Yan X, Liu F, Wang X. Experimental study on energy conversion of flow induced motion for two triangular prisms in staggered arrangement. Energy 2022;249:123764.
[26] Kim ES, Bernitsas MM. Performance prediction of horizontal hydrokinetic energy converter using multiple-cylinder synergy in flow induced motion. Appl Energy 2016;170:92–100.
[27] Zhao J, Hourigan K, Thompson MC. Dynamic response of elliptical cylinders undergoing transverse flow-induced vibration. J Fluids Struct 2019;89:123–31.
[28] Shi G, Tan T, Hu S, Yan Z. Hydrodynamic piezoelectric energy harvesting with topological strong vortex by forced separation. Int J Mech Sci 2022;223:107261.
[29] Lo JCC, Hourigan K, Thompson MC, Zhao J. The effect of structural damping on flow-induced vibration of a thin elliptical cylinder. J Fluid Mech 2023;974:A5.
[30] Soti AK, Zhao J, Thompson MC, Sheridan J, Bhardwaj R. Damping effects on vortex-induced vibration of a circular cylinder and implications for power extraction. J Fluids Struct 2018;81:289–308.
[31] Zhao J, Hourigan K, Thompson M. Flow-induced vibration of D-section cylinders: an afterbody is not essential for vortex-induced vibration. J Fluid Mech 2018;851:317–43.
[32] Zhao J, Lo Jacono D, Sheridan J, Hourigan K, Thompson MC. Experimental investigation of in-line flow-induced vibration of a rotating circular cylinder. J Fluid Mech 2018;847:664–99.
[33] Sumer BM, et al. Hydrodynamics around cylindrical structures. In: Advanced series on ocean engineering, vol. 26, World Scientific; 2006.
[34] Khalak A, Williamson C. Dynamics of a hydroelastic cylinder with very low mass and damping. J Fluids Struct 1996;10(5):455–72.
[35] Zhao J, Leontini JS, Lo Jacono D, Sheridan J. Fluid–structure interaction of a square cylinder at different angles of attack. J Fluid Mech 2014;747:688–721.
[36] Lee J, Bernitsas M. High-damping, high-Reynolds VIV tests for energy harnessing using the VIVACE converter. Ocean Eng 2011;38(16):1697–712.
[37] Wang J, Zhao W, Su Z, Zhang G, Li P, Yurchenko D. Enhancing vortex-induced vibrations of a cylinder with rod attachments for hydrokinetic power generation. Mech Syst Signal Process 2020;145:106912.
[38] Wang Z, Du L, Zhao J, Sun X. Structural response and energy extraction of a fully passive flapping foil. J Fluids Struct 2017;72:96–113.
[39] Kinsey T, Dumas G. Parametric study of an oscillating airfoil in a power-extraction regime. Am Inst Aeronaut Astronaut J 2008;46(6):1318–30.
[40] Manwell JF, McGowan JG, Rogers AL. Wind energy explained: theory, design and application. 2nd ed. John Wiley & Sons; 2011, p. 137.
[41] Burton T, Jenkins N, Sharpe D, Bossanyi E. Wind energy handbook. John Wiley & Sons; 2011.
[42] Wilson R, Lissaman P, Walker S. Aerodynamic performance of wind turbines. Tech. rep., Corvallis (USA): Oregon State Univ.; 1976.
[43] Wang J-S, Fan D, Lin K. A review on flow-induced vibration of offshore circular cylinders. J Hydrodyn 2020;32(3):415–40.
[44] Chang C-C, Bernitsas MM. Hydrokinetic energy harnessing using the VIVACE converter with passive turbulence control. In: International conference on offshore mechanics and arctic engineering, vol. 44373. 2011, p. 899–908.